Topological phases of Bi(111) bilayer in an external exchange field

Hongbin Zhang,* Frank Freimuth, Gustav Bihlmayer, Stefan Blügel, and Yuriy Mokrousov
Peter Grünberg Institut and Institute for Advanced Simulation, Forschungszentrum Jülich and JARA, D-52425 Jülich, Germany
(Received 22 March 2012; revised manuscript received 16 May 2012; published 5 July 2012)

Using first-principles methods, we investigate topological phase transitions as a function of exchange field in a Bi(111) bilayer. Evaluation of the spin Chern number for different magnitudes of the exchange field reveals that when the time-reversal symmetry is broken by a small exchange field, the system enters the time-reversal broken topological insulator phase, introduced by Yang *et al*. [Phys. Rev. Lett. **107**, 066602 (2011)]. After a metallic phase in the intermediate region, the quantum anomalous Hall phase with a nonzero Chern number emerges at a sufficiently large exchange field. We analyze the phase diagram from the viewpoint of the evolution of the electronic structure, edge states, and transport properties and demonstrate that different topological phases can be distinguished by the spin polarization of the edge states as well as spin or charge transverse conductivity.

DOI: 10.1103/PhysRevB.86.035104 PACS number(s): 75.70.−i, 73.20.At, 75.30.Kz

I. INTRODUCTION

Topological insulators (TIs) have drawn quite intensive attention recently owing to the gapless surface/edge states, topologically protected against perturbations which do not close the bulk gap.[1,2] Similar to graphene,[3] exciting physical properties are expected if the TI surface/edge states are made gapped, resulting in, e.g., a half-quantized surface Hall effect,[4] topological magnetoelectric effects,[5,6] and Majorana zero states.[7] It is suggested that such effects can be triggered via the proximity effect of TIs to magnetically ordered materials or superconductors, in which case new terms which impose or break certain symmetries are introduced into the effective Hamiltonian.

One particularly interesting situation arises if the time-reversal symmetry $\mathcal{T}$ in a TI is broken via a controlled perturbation. The definition of the $\mathbb{Z}_2$ topological invariant, used to classify two-dimensional (2D) insulators into ordinary insulators and TIs, hinges on the presence of the time-reversal symmetry in the system.[8] It still remains an open question of how to generalize the $\mathbb{Z}_2$ topological invariant when $\mathcal{T}$ is broken. In such a case, it is suggested[9] that it is plausible to use the so-called spin Chern number:[10]

$$\mathcal{C}_s = \tfrac{1}{2}(\mathcal{C}_+ - \mathcal{C}_-), \tag{1}$$

where $\mathcal{C}_+$ and $\mathcal{C}_-$ are the Chern numbers for the spin "up" and "down" manifolds of the occupied states. Since the spin-orbit coupling (SOC) in general induces spin mixing, the spin Chern number is well defined only when the system exhibits a gap in the spectrum of σ_z in addition to being a band insulator. In this case $\mathcal{C}_s$ proves to be equivalent to the $\mathbb{Z}_2$ number when time-reversal symmetry is present.[11] For models of TIs[10] and graphene,[9] the spin Chern number picture proved to be valid, while a more detailed analysis of this concept in real materials investigated from first principles is still lacking.

Owing to $\mathcal{T}$ symmetry, the surface/edge states of TIs are spin degenerate, making it hard to manipulate and exploit their transport properties in experiments based on magnetic detection. While the quantum Hall effect usually requires a very large magnetic field to emerge, in this sense, the quantum anomalous Hall (QAH) effect in ferromagnets would be much more suited for future spintronics. The QAH effect, which has attracted a lot of attention recently but so far has not been verified experimentally, occurs in 2D Chern insulators[12] with broken $\mathcal{T}$ symmetry, exhibiting overall spin-polarized edge states carrying a quantized electric charge. Up to now, it has been believed that TIs can be turned into Chern insulators via magnetic doping,[13,14] but it still remains an experimentally unsolved problem despite recent advances in this direction.[15,16] In this light, it is necessary to explore how tunable 2D TIs are under $\mathcal{T}$-broken perturbations, in particular, exchange interactions.

Bismuth is the heaviest atom with an effectively stable isotope,[17] and strong spin-orbit coupling makes it an important ingredient of the newly discovered TIs such as Bi_2Se_3[18] and $Bi_{1-x}Sb_x$.[8] Ultrathin Bi(111) films, which can be produced experimentally on different substrates,[19,20] are also predicted to be 2D TIs.[21–23] In our study we take the Bi(111) bilayer as a representative of the latter class of TIs. In this work, we investigate the topological phase transitions in a 2D TI, the Bi(111) bilayer,[21] in an external exchange field using first-principles methods. We found that at small exchange fields the bilayer is in the time-reversal broken topological insulator phase, which can be characterized by nontrivial values of spin Chern numbers, transverse spin Hall conductivity, and spin polarization of the edge states. Increasing the magnitude of the exchange field further drives the system first into a metal and then into a QAH phase. Detailed analysis of the electronic structures reveals that spin mixing is important for closing the bulk gap and Chern number exchange between valence and conduction bands. Finally, we analyze the spin polarization of the metallic edge states in different phases, show that its sign can be controlled by the strength of the exchange field, and prove that its magnitude is large enough to be observed in scanning tunneling microscopy experiments.

II. METHOD

In a Bi(111) bilayer two layers of Bi atoms form a honeycomb lattice when projected onto the plane of the film. The relaxed bulk in-plane lattice constant and the distance between the two layers were 4.52 and 1.67 Å, respectively (see also Fig. 4). Our theoretical investigations are based on density functional theory.[24] We apply the local-density approximation[25] to the exchange-correlation potential and use

the full-potential linearized augmented-plane-wave method (FLAPW) as implemented in the FLEUR code.[26] The self-consistent calculations with SOC were carried out with a cutoff parameter $k_{\max}$ of 3.8 bohr^{-1} and 50 k points in the full two-dimensional Brillouin zone (BZ). A muffin-tin radius of 2.5 Bohr was used. The band structure of the system with SOC is presented in Fig. 2(f). The Wannier function technique was used on top of self-consistent DFT calculations to derive an accurate tight-binding Hamiltonian for the system.[27–29] Moreover, we have constructed the matrix elements $\langle \psi_{m\mathbf{k}} \mid \sigma_\alpha \mid \psi_{n\mathbf{k}} \rangle$ of the Pauli matrices σ_α ($\alpha = x,y,z$), where $\psi_{n\mathbf{k}}$ are the occupied Bloch wave functions. These matrices were evaluated from the DFT calculations and transformed into the real-space representation in terms of maximally localized Wannier functions (MLWFs).[29] This allowed us to take into account an exchange field applied perpendicularly to the surface of the bilayer by adding a $\sigma_z \cdot B$ term on top of the original Hamiltonian and provided an ability to accurately evaluate spin polarization P_α (see the caption of Fig. 4 for details). In general, applying an exchange field lifts the spin degeneracy, where spin-up (spin-down) states get higher (lower) in energy spectra, and the difference of the occupation of spin-up and spin-down leads to the spin polarization P_α, which can be positive (negative) along the direction of exchange fields. In Figs. 2(a)–2(e), 2(k)–2(o), and 4, spin-up (minority) and spin-down (majority) states are indicated in red and blue, respectively.

For a band insulator the transverse anomalous Hall conductivity (AHC) is $\frac{e^2}{h}$ times the conventional integer (first) Chern number, where[30]

$$\mathcal{C} = \mathcal{C}_+ + \mathcal{C}_- = -\frac{1}{2\pi} \sum_{n=1}^{occ} \int d^2k\, \Omega_n^{xy}(\mathbf{k}), \qquad (2)$$

in which the summation goes over all occupied states and $\Omega_n(\mathbf{k})$ is the Berry curvature of the nth band, given by

$$\Omega_n^{xy}(\mathbf{k}) = -2\mathrm{Im}\left\langle \frac{\partial u_{n\mathbf{k}}}{\partial k_x} \middle| \frac{\partial u_{n\mathbf{k}}}{\partial k_y} \right\rangle = -2\mathrm{Im} \sum_{m \neq n} \frac{\langle u_{n\mathbf{k}} \mid \hat{v}_x \mid u_{m\mathbf{k}} \rangle \langle u_{m\mathbf{k}} \mid \hat{v}_y \mid u_{n\mathbf{k}} \rangle}{(\epsilon_{n\mathbf{k}} - \epsilon_{m\mathbf{k}})^2}, \qquad (3)$$

where $u_{n\mathbf{k}}$ is the lattice-periodic part of $\psi_{n\mathbf{k}}$ with energy eigenvalues $\epsilon_{n\mathbf{k}}$ and $\hat{v}_\nu$ ($\nu = x,y$) is the velocity operator. To evaluate the spin Hall conductivity, we have replaced $\hat{v}_x$ with the spin-velocity operator $\hat{s}_x^z = \{\hat{v}_x, \sigma_z\}$ in Eq. (3).

To calculate the spin Chern number, we followed the procedure of Ref. 10. First, the σ_z matrix for the occupied states $\langle \psi_{m\mathbf{k}} \mid \sigma_z \mid \psi_{n\mathbf{k}} \rangle$ (m, n are the band indices of occupied states at each $\mathbf{k}$) is constructed and diagonalized. Note that due to the spin-flip part of the spin-orbit coupling,[31] the eigenvalues of the σ_z matrix are not necessarily ± 1. Then, using the spin-up or spin-down eigenvectors $|\phi^\pm\rangle$ of the σ_z matrix, the occupied states are projected into the spin-up and spin-down manifolds $\psi^\pm = \langle \phi^\pm(\mathbf{k}) \mid \psi(\mathbf{k}) \rangle$, where $|\psi(\mathbf{k})\rangle$ denotes the eigenvector of the occupied states. Finally, the spin Chern number is evaluated by integration of the Berry curvature for each manifold where the derivatives of the wave functions $\psi^\pm$ with respect to $\mathbf{k}$ are obtained using the finite difference methods.[32] The spin Chern number is well defined only if the spectrum of σ_z is gapped.[10] In our calculations, we observed that in the range of exchange field considered (0 eV $\leqslant B \leqslant$ 1 eV) the spectrum of σ_z remains finite, which justifies the usage of spin Chern numbers in this work.

III. CHERN NUMBERS AND THE PHASE DIAGRAM

Here, we calculate the Chern numbers and analyze the topological phases of the Bi(111) bilayer as a function of the externally added exchange field B, presenting the phase diagram, calculated band gap, and AHC in Fig. 1. When $B = 0$, the system is a 2D TI with a $\mathbb{Z}_2$ number of 1 (nontrivial). The Chern numbers for the spin-up (minority) and spin-down (majority) manifolds are $\mathcal{C}_\pm = \mp 1$, respectively, leading to a spin Chern number $\mathcal{C}_s = -1$ [cf. Eq. (1)], in agreement with previous calculations.[22] In this case, the spin Chern number is equivalent to the $\mathbb{Z}_2$ number. Introducing and increasing the exchange field breaks the $\mathcal{T}$ symmetry and causes an exchange splitting between the spin-up and spin-down valence and conduction bands, bringing thus the minority valence bands towards majority conduction bands[33] [Fig. 2(b)]. A further increase of the exchange field leads to a closure of the gap at $B = 0.31$ eV [Fig. 2(c)]. As evident from Figs. 2(a)–2(c), until the bulk gap is closed, the original inverted band structure at the Γ point remains topologically nontrivial. This is confirmed by calculating the spin Chern number $\mathcal{C}_\pm = \mp 1$ for $0 \leqslant B \leqslant 0.31$ eV, identifying the topological phase of the Bi(111) bilayer in this range of the exchange field as the $\mathcal{T}$-broken (TRB) TI phase (c.f. Fig. 1), analogous to that considered in graphene.[9]

To verify that the $\mathcal{T}$-broken phase could display nontrivial topological transport properties, we calculate the transverse spin Hall conductivity (SHC) as a function of the spin-orbit strength in the system λ and present the results in Fig. 3. Consider first the bilayer at $B = 0$. At small SOC strength the system is in a trivial insulator phase, which can be characterized with a zero SHC. Upon increasing λ, the bilayer first goes through a metallic phase, and at around

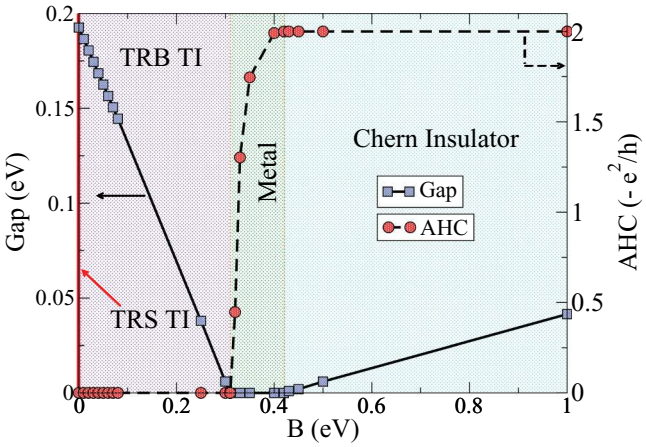

FIG. 1. (Color online) Phase diagram of the Bi(111) bilayer with respect to the exchange field B. Blue squares (red circles) mark the band gap (anomalous Hall conductivity) as a function of B. Regions of different topological phases, namely, $\mathcal{T}$-conserved TI (TRS TI), $\mathcal{T}$-broken TI (TRB TI), metal, and Chern insulator (QAH) are shaded differently and labeled accordingly.

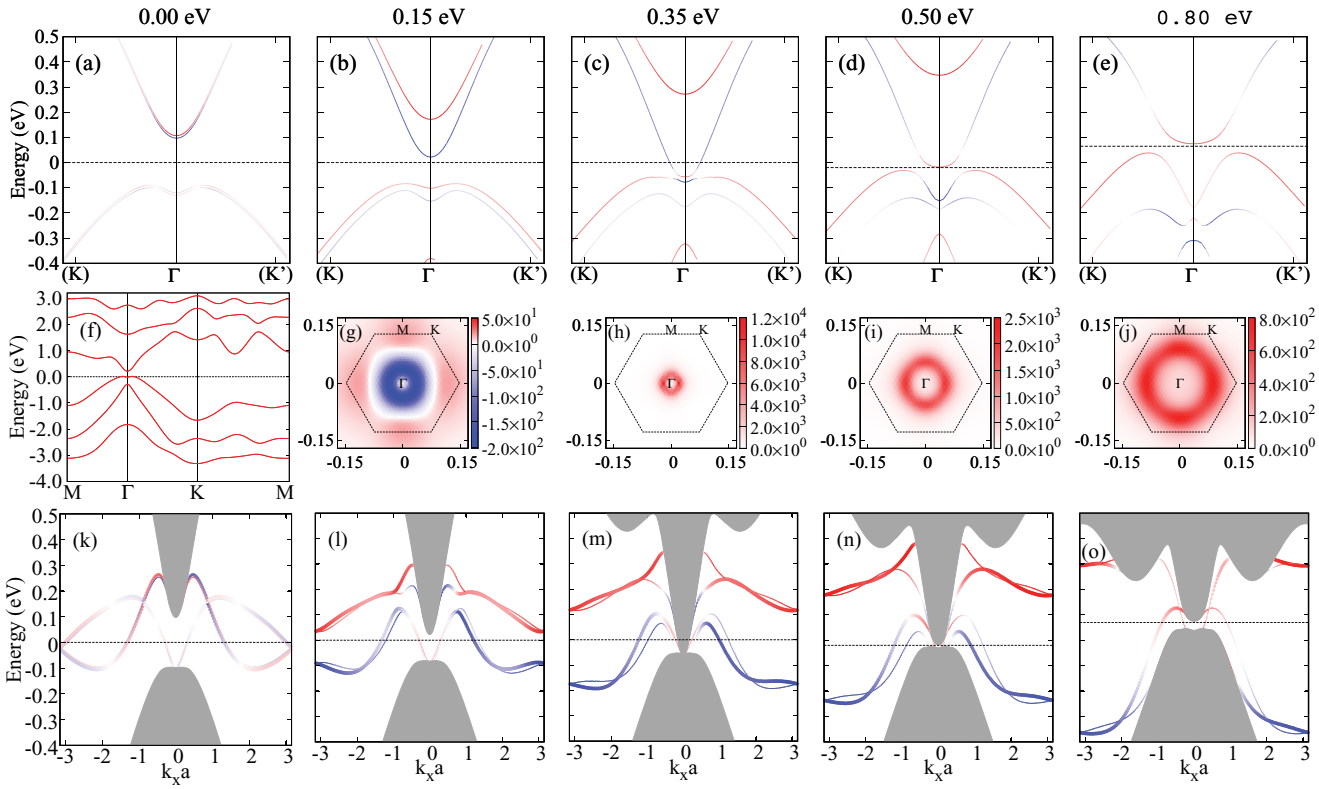

FIG. 2. (Color online) Electronic structure of Bi(111) bilayer in an external exchange field perpendicular to the surface. (a)–(e) display the 2D bulk band structure for an exchange field of 0.0, 0.15, 0.35, 0.5, and 0.8 eV (indicated at the top), respectively. Red (blue) stands for positive (negative) spin polarization along the field of the states in arbitrary units. The band structures are plotted along the K-Γ-K' path in the vicinity of the Γ point. In (a) the spin-up states are shifted by 10 meV upwards in energy to make the degeneracy of the states more visible. In (f) the 2D bulk band structure of the Bi(111) bilayer is displayed. Each band is doubly degenerate. (g)–(j) display the distribution of the Berry curvature of occupied states in the BZ (to a minus sign) with the exchange field marked on the top. Blue (red) indicates positive (negative) values of the Berry curvature (in a.u.^{2}). The evolution of the band structure of an 80-atom wide zigzag ribbon is shown in (k)–(o). Edge states are colored with the expectation value of the σ_z, rendered in blue and red for negative and positive values, respectively. The size of the points indicates the weight from atoms located on the upper edge of the ribbon. The gray shaded regions denote the projected 2D bulk band structure from the 2D BZ onto the 1D k vector of the ribbon. In (k) the spin-up states are shifted by 10 meV upwards in energy to make the degeneracy of the states more visible. Horizontal dotted lines in (a)–(e) and (k)–(o) indicate the constant energies (chosen to be in the bulk gap in insulating phases) for which the spin polarization is analyzed as shown in Fig. 4.

70% ($\lambda = 0.7$) of the SOC strength of Bi atoms a transition to the TI phase with a SOC-driven band inversion occurs, which is accompanied by a nonzero SHC of the magnitude of around $-0.7\frac{e}{4\pi}$.[22] The deviation from the quantized value of $-\frac{e}{4\pi}$ is due to the nonvanishing spin-nonconserving part of the spin-orbit interaction: artificially switching it off in our calculations,[31] we indeed acquire a quantized value of $-\frac{e}{4\pi}$ for the SHC (dashed line in Fig. 3), in accordance with the original scenario proposed first for HgTe/(Hg,Cd)Te quantum spin Hall heterostructures.[34–36] By looking at the SHC for the Bi bilayer at $B = 0.15$ eV, we observe an almost identical behavior to that without the field, with modifications only in the boundaries of the metallic region, SHC in the metallic regime, and a slight difference in the value of the SHC at large λ. Again, by neglecting the spin-nonconserving part of the SOC, we restore a quantized value of $-\frac{e}{4\pi}$ for the SHC in the TRB TI phase, which clearly manifests a topologically nontrivial phase, as far as the topological transport is concerned. Note that for both phases, TI and TRB TI, the transverse charge conductivity in exactly zero when λ lies outside of the metallic region. The ability to characterize the $\mathcal{T}$-broken TI phase by an experimentally observable nonzero spin Hall conductivity could be particularly important for distinguishing this phase from a trivial insulator since, as we shall see in the next section, the topological protection of the edge states in the system for $B \neq 0$ is lifted.

Returning now to the phase diagram in Fig. 1, we observe that the size of the band gap decreases linearly as the exchange field is increased, and for B in between 0.31 and 0.42 eV the bulk gap is closed with the Bi(111) bilayer in the metallic phase [see Fig. 1]. However, increasing the exchange field further reopens the gap, which results in the occurrence of a topologically nontrivial phase. For $B \geqslant 0.42$ eV the spin Chern number of the occupied majority states reverses sign, leading to a zero spin Chern number $\mathcal{C}_s$, while the Chern number $\mathcal{C}$ acquires a value of -2. That is, in this range of the exchange field the system is in the QAH, or Chern insulator phase. It is worth recalling here that in the case of a metal in which the spin-nonconserving part of the spin-orbit interaction is hypothetically switched off,[31] the intrinsic anomalous Hall

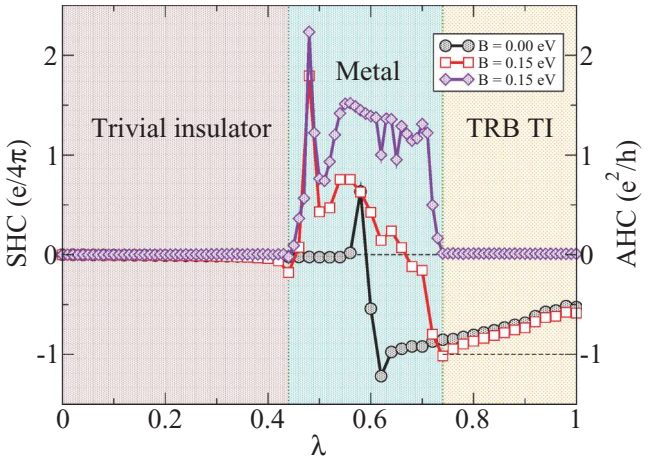

FIG. 3. (Color online) Spin Hall conductivity and anomalous Hall conductivity of the Bi(111) bilayer with respect to the scaled strength of the spin-orbit coupling of Bi atoms λ. λ = 1 corresponds to the unscaled SOC strength. Black circles (red squares) denote the SHC with $B = 0.0$ eV ($B = 0.15$ eV), while purple diamonds mark the AHC with $B = 0.15$ eV. The horizontal dashed line at SHC = $-\frac{e}{4\pi}$ stands for the quantized magnitude of the SHC if the spin-flip part of the SOC is switched off.

conductivity is given by the sum of the Hall conductivities for spin-up and spin-down bands, while the spin Hall conductivity is given by their difference (spin is a good quantum number in such a case).[31,37] Evidently, such a correspondence between the Chern number and the spin Chern number, i.e., their representation as the sum and the difference of the Chern numbers for spin-up and spin-down bands, holds true for the Bi(111) bilayer with a gapped spectrum of σ_z, based on the argument that a unitary transformation (eigenvectors of σ_z in our case) of the occupied states will keep the Chern number invariant.[38]

Examining the electronic structure of the system, presented in Fig. 2, reveals that it is the spin mixing accompanied by the exchange of the Chern number between valence and conduction bands that leads to the phase transition from the $\mathcal{T}$-conserved TI phase to the QAH phase through the $\mathcal{T}$-broken TI and metallic phases. The occurrence of the metallic phase has not been predicted previously, e.g., for graphene[9] or Bi_2Se_3.[39] It emerges due to an overlap in energy of bands with opposite spin character in the vicinity of the Γ point [cf. Fig. 2(c)], which is characteristic of a material with a nonmonotonous dispersion of the bands on both sides of the Γ point. Such a metallic phase cannot be achieved, e.g., for pure Dirac bands, which have a local maximum (minimum) at the high symmetry (in this case) Γ point, as is evident from Fig. 2(c).

Our transport calculations according to Eq. (3) show that a finite AHC develops in the metallic and QAH phases; see Fig. 2. Microscopically, the nonvanishing AHC can be traced back to the development of the singular Berry curvature in k space as the B field is increased; see Figs. 2(g)–2(j). For B below 0.31 eV the Berry curvature has a nontrivial distribution in the BZ with the regions of positive and negative values of comparatively small magnitude [Fig. 2(g)], while the BZ integral of the Berry curvature amounts to zero.

At the onset of the metallic phase there is a noticeable hybridization between the conduction and valence bands of opposite spin, which gives rise to a very large negative contribution to the Berry curvature around the points in the BZ at the Fermi level E_F, where the orbital character and the spin character of the valence and conduction bands are changing, or, in the terminology of Ref. [31], along a "hot loop" in the BZ [Figs. 2(c)–2(e) and 2(h)–2(j)]. In such a situation, the Berry curvature and the AHC, which is proportional to the integrated value of the Berry curvature over the BZ, are dominated by the spin-flip transitions mediated by the non-spin-conserving part of the spin-orbit interaction.[31] At the Γ point, the sign of the Berry curvature reverses for $B > 0.3$ eV, accompanying the switch in parity of the valence and conduction bands.

In the metallic phase, the AHC as a function of B is monotonously increasing (Fig. 1), while the radius of the hot loop is increasing owing to the shift of the hybridization point between the valence and conductance bands away from Γ (Fig. 2). When the gap is reopened for $B > 0.42$ eV, the AHC reaches a value of $-2\frac{e^2}{h}$, with Chern number $\mathcal{C} = -2$; see Fig. 2. In the QAH phase, we observe from our calculations that, out of six valence bands, the two topmost bands dominate the contribution to the AHC for exchange fields up to 0.60 eV. When the exchange field is increased further, deeper spin-up bands will be pushed closer to the Fermi energy and take the spin-down character derived from the conduction bands [cf. Fig. 1(e)], also providing a contribution to the Berry curvature.

IV. EDGE STATES

We turn now to the properties of the edge states in the Bi(111) bilayer zigzag ribbon with a width of 80 atoms in the y direction and that is periodic (infinite) in the x direction.[21] The tight-binding Hamiltonian of the ribbon was constructed in terms of the MLWFs by a mere termination of the 2D (infinite) Hamiltonian after 40 unit cells in the y direction. For the Bi(111) ribbon, when $\mathcal{T}$ symmetry is not broken, there are 12 edge states in total, as evident from Fig. 2(k). Six of them are located on each side of the ribbon, while out of these six there are three spin-up left movers and three spin-down right movers. The axis of spin polarization of the edge states is determined by the details of the electronic structure and spin-orbit interaction and can be also energy dependent.[22]

Applying the exchange field to the ribbon breaks the $\mathcal{T}$ symmetry, lifts the spin degeneracy, and polarizes the edge states along the direction of the applied field [see Figs. 2(l)–2(o)]. A close inspection of the edge bands in the case of the TRB TI phase [Fig. 2(l)] reveals that the edge states do not connect the valence and conduction bands in the system, as in the case of the edge states of a conventional TI [cf. Fig. 2(k)]. This means that the Hamiltonian of the system can be transformed such that the spectrum at the edges exhibits a gap at the Fermi energy. Moreover, owing to the breaking of the $\mathcal{T}$ symmetry, backscattering is, in general, allowed, which results in the dissipative transport properties of the edge states.[9] Noticeably, in the QAH phase [Figs. 2(n) and 2(o)] the connection of the valence and conduction bands of the bilayer via the edge states is restored again, resulting in a dissipationless longitudinal transport of the ribbon, realized by the topologically protected edge states.

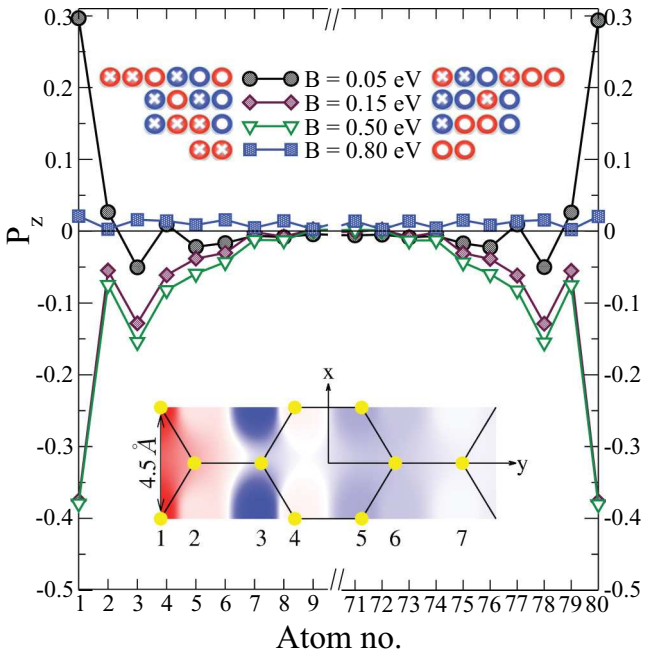

FIG. 4. (Color online) Spatial distribution of the spin polarization P_z at the Fermi energy of the edge states in a zigzag Bi(111) ribbon with a width of 80 atoms. P_z is obtained as a sum of the expectation values of σ_z for all edge states at the constant energies [marked with dashed lines in Figs. 2(a)–2(e)], multiplied by the weight of the corresponding wave function on the given atom. The structure of the edge states on each side of the ribbon is marked with circles to the left (left edge) and to the right (right edge) of the value of the corresponding exchange field B. While the direction of propagation of the edge states is marked with white dots (white crosses) for the direction towards the reader (away from the reader), red (blue) circles mark the predominantly spin-up (spin-down) character of the edge states. The bottom inset depicts the distribution of P_z for $B = 0.05$ eV (in arbitrary units, with red for positive and blue for negative values) along and across the ribbon, where yellow spheres stand for the positions of Bi atoms.

Of particular interest here is the spatial distribution of the spin polarization of the edge states around the Fermi energy, P_z, which plays a very important role in spin-polarized scanning tunneling microscopy (SP-STM) experiments.[40] We calculate this spin polarization as a function of the B field in real space across the ribbon and present the results in Fig. 4. Let us consider first the case of a very small exchange field $B = 0.05$ eV and look at the spin polarization at E_F across the ribbon (Fig. 4). We observe that the spin polarization (i) is rather localized at the edges of the ribbon, (ii) reaches very large values, and (iii) displays oscillations in sign across the ribbon. These properties can be understood by referring to the electronic structure of the edge states for this value of the field, which is quite similar to that depicted in Fig. 2(l), only with the smaller separation between the upper (predominantly spin-up) and lower (predominantly spin-down) subgroups of two edge states, so that there are 12 states at E_F all together. The direction and spin character of the edge states at E_F are sketched in Fig. 4. We observe that owing to the presence of the nonzero exchange field and breaking of $\mathcal{T}$ symmetry, the edge states get spin polarized, while on each side of the ribbon the number of right and left movers is equal for $B < 0.42$. This results in zero transverse charge conductance, in accordance with the phase diagram (Fig. 1).

For larger wave vectors $|k_x \cdot a| \approx \pi$ [see Fig. 2(l)], the upper group of two states has a strong spin-up character, and for $B = 0.05$ eV (not shown) it crosses the Fermi energy, giving rise to a strong spin polarization in the direction of the B field. Since the states with larger k_x (away from the bulk bands) are more localized at the edges of the ribbon than the states with smaller k_x (closer to the bulk bands),[21] positive P_z in Fig. 4 for this field is localized at the ribbon edges. Correspondingly, the states at E_F close to Γ are the source of negative spin polarization, which is smeared more across the ribbon owing to stronger hybridization with the bulk states, thus giving rise to the change in the sign of P_z away from the ribbon edges. We speculate that such oscillatory spatial dependence of P_z should be a common phenomenon in a situation where the electronic structure of the edge states of a 2D TI exposed to an exchange field is nontrivial. The spatial distribution of the P_z in the unit cell for this case is illustrated in the inset of Fig. 4.

Increasing the exchange field further pushes the tail of long-wavelength spin-up edge states out of the bulk gap completely around $B = 0.15$ eV [Fig. 2(l)]. In this case, there are only eight edge states left, whose direction of the spin polarization at the Fermi energy is opposite to the direction of the B field. Since the Bi(111) bilayer exhibits a $\mathcal{T}$-broken TI phase for this value of B, there are two left and two right movers on each side of the ribbon, with zero transported charge [Fig. 4]. In correspondence to the predominantly spin-down character of the edge states in k space, P_z is large and negative in the vicinity of the edge of the ribbon. Noticeably, the spin polarization decays much slower with the distance towards the center of the ribbon, when compared to the case considered previously, owing to the proximity of the edge states in k space to the bulk states. We remark here that the predicted change in sign of P_z is an interesting phenomenon, which can be exploited experimentally, e.g., via tuning the strength of the exchange field by deposition of different adatoms[39,41] (see also comments in Sec. V).

The evolution of the edge states for $0.15 \leqslant B \leqslant 0.80$ eV can be seen in Figs. 2(l)–2(o). As the exchange field is increased, the magnitude of P_z gradually decreases since the conduction and valence bands become very close in energy, and the k_F vectors of the edge states approach the Γ point. This is particularly clear for the edge states in the QAH phase at $B = 0.8$ eV, for which P_z and its decay rate into the ribbon are very small (Fig. 4). For the regime of B in between 0.42 and 0.7 eV, i.e., at the onset of the QAH phase, the number of edge states is the same as that in the $\mathcal{T}$-broken TI phase at $B = 0.15$ eV, but the emergent quantized charge conductance of the edge states proportional to $\mathcal{C}$ on each side of the ribbon is evident (Fig. 4). When $B > 0.7$ eV four more edge states are pushed out of the bulk gap window, and only four edge states crossing E_F are left overall. In this case, we have a situation of two right/left movers on each side of the ribbon, with a small positive spin polarization (Fig. 4). The microscopic mechanism for spin-polarized electron conduction in these edge states without the possibility to backscatter remains an open and interesting topic for future studies.

V. SUMMARY

In this work, based on first-principles calculations, we have considered the emerging topological phases of the Bi(111) bilayer in an external exchange field B. We identify four different phases as the exchange field is varied: the TI phase for $B = 0$, the $\mathcal{T}$-broken TI phase for small fields, the metallic phase for intermediate fields, and the Chern insulator, or QAH, phase for large exchange fields. We consistently identify each of the insulating phases in terms of the Chern number $\mathcal{C}$, spin Chern number $\mathcal{C}_s$, spin, and charge transverse conductivity. We attribute the origin of the phase transitions to the spin-orbit mediated spin mixing between the valence and conduction bands whose topology in k space is controlled by the applied field.

In particular, we focus on the electronic structure and development of the edge states in a zigzag ribbon of the Bi(111) bilayer as a function of the B field. We show that the spin polarization of the edge states along the direction of the exchange field at the Fermi level can be significant in magnitude, and its sign as well as its spatial distribution can be controlled by changing the magnitude of the applied field. Since reversing the direction of the exchange field leads to a reversed propagation direction and a reversed spin polarization of the edge states, the exchange field provides a tool to tune the properties of one-dimensional spin-polarized transport arising at the edges of insulators with nontrivial topological properties. We also speculate that the spin polarization of the edge states, which characterizes different topological phases, can be observed in, e.g., scanning tunneling microscopy experiments.

We remark that the experimental realization of the tunable exchange field applied to a thin Bi(111) bilayer can be sought in two directions. One way lies in finding a suitable insulating substrate for deposition of Bi(111) which exhibits essential magnetism at least at the interface with the bilayer. In this case the direction of the B field can be easily (depending on the magnetocrystalline anisotropy energy) reversed, while the magnitude of the exchange field can be tuned via, e.g., the magnetoelectric effect if the substrate used for deposition has multiferroic properties. The second route lies in deposition of transition metal adatoms on the Bi(111) surface. Recently, it has been demonstrated theoretically that such adatom deposition can induce considerable exchange splitting with a magnitude as large as several tenths of eV on the topological insulator underneath,[41] and for Bi_2Se_3, the exchange field is large enough to get the system into the QAH phase.[39] The magnitude of the exchange field in this case can be controlled by an appropriate choice of the transition metal or by deposition of the system on an insulating nonmagnetic substrate, which can cause essential modifications in the distance between the TI and deposited adatoms. We also note that, generally speaking, the magnitude of the exchange field necessary to achieve the QAH phase in the phase diagram of Fig. 1 depends directly on the initial value of the gap in the TI phase without the field.

ACKNOWLEDGMENTS

We acknowledge very helpful discussions with Emil Prodan, Sheng Li, Klaus Koepernik, and Marjana Ležaić. This work was supported by the HGF-YIG Programme VH-NG-513 and by the DFG through Research Unit 912 and Grant No. HE3292/7-1. Computational resources were provided by the Jülich Supercomputing Centre.

*Corresponding author: h.zhang@fz-juelich.de

[1] M. Z. Hasan and C. L. Kane, Rev. Mod. Phys. **82**, 3045 (2010).
[2] X.-L. Qi and S.-C. Zhang, Rev. Mod. Phys. **83**, 1057 (2011).
[3] A. H. Castro Neto, F. Guinea, N. M. R. Peres, K. S. Novoselov, and A. K. Geim, Rev. Mod. Phys. **81**, 109 (2009).
[4] X.-L. Qi, T. L. Hughes, and S.-C. Zhang, Phys. Rev. B **78**, 195424 (2008).
[5] X.-L. Qi, R. Li, J. Zang, and S.-C. Zhang, Science **323**, 1184 (2009).
[6] A. M. Essin, J. E. Moore, and D. Vanderbilt, Phys. Rev. Lett. **102**, 146805 (2009).
[7] L. Fu and C. L. Kane, Phys. Rev. Lett. **100**, 096407 (2008).
[8] L. Fu and C. L. Kane, Phys. Rev. B **76**, 045302 (2007).
[9] Y. Yang, Z. Xu, L. Sheng, B. Wang, D. Y. Xing, and D. N. Sheng, Phys. Rev. Lett. **107**, 066602 (2011).
[10] E. Prodan, Phys. Rev. B **83**, 195119 (2011).
[11] E. Prodan, New. J. Phys. **12**, 065003 (2010).
[12] F. D. M. Haldane, Phys. Rev. Lett. **61**, 2015 (1988).
[13] C.-X. Liu, X.-L. Qi, X. Dai, Z. Fang, and S.-C. Zhang, Phys. Rev. Lett. **101**, 146802 (2008).
[14] R. Yu, W. Zhang, H.-J. Zhang, S.-C. Zhang, X. Dai, and Z. Fang, Science **329**, 61 (2010).
[15] C.-Z. Chang, J.-S. Zhang, M.-H. Liu, Z.-C. Zhang, X. Feng, K. Li, L.-L. Wang, X. Chen, X. Dai, Z. Fang, X.-L. Qi, S.-C. Zhang, Y. Wang, K. He, X.-C. Ma, and Q.-K. Xue, arxiv:1108.4754.
[16] K. S. Novoselov, A. K. Geim, S. V. Morozov, D. Jiang, M. I. Katsnelson, I. V. Grigorieva, G. V. Dubonos, and A. A. Firsov, Nature (London) **438**, 197 (2005).
[17] P. de Marcillac, N. Coron, G. Dambier, J. Leblanc, and J.-P. Moalic, Nature **422**, 876 (2003).
[18] Y. Xia, D. Qian, D. Hsieh, L. Wray, A. Pal, H. Lin, A. Bansil, D. Grauer, Y. S. Hor, R. J. Cava, and M. Z. Hasan, Nat. Phys. **5**, 398 (2009).
[19] T. Nagao, J. T. Sadowski, M. Saito, S. Yaginuma, Y. Fujikawa, T. Kogure, T. Ohno, Y. Hasegawa, S. Hasegawa, and T. Sakurai, Phys. Rev. Lett. **93**, 105501 (2004).
[20] T. Hirahara, G. Bihlmayer, Y. Sakamoto, M. Yamada, H. Miyazaki, S. I. Kimura, S. Blugel, and S. Hasegawa, Phys. Rev. Lett. **107**, 166801 (2011).
[21] M. Wada, S. Murakami, F. Freimuth, and G. Bihlmayer, Phys. Rev. B **83**, 121310(R) (2011).
[22] S. Murakami, Phys. Rev. Lett. **97**, 236805 (2006).
[23] Z. Liu, C.-X. Liu, Y.-S. Wu, W.-H. Duan, F. Liu, and J. Wu, Phys. Rev. Lett. **107**, 136805 (2011).
[24] P. Hohenberg and W. Kohn, Phys. Rev. **136**, B864 (1964).
[25] V. L. Moruzzi, J. F. Janak, and A. R. Williams, *Calculated Properties of Metals* (Pergamon, New York, 1978).
[26] For a description of the code [see http://www.flapw.de].

[27]X. Wang, J. R. Yates, I. Souza, and D. Vanderbilt, Phys. Rev. B **74**, 195118 (2006).
[28]F. Freimuth, Y. Mokrousov, D. Wortmann, S. Heinze, and S. Blügel, Phys. Rev. B **78**, 035120 (2008).
[29]A. A. Mostofi, J. R. Yates, Y.-S. Lee, I. Souza, D. Vanderbilt, and N. Marzari, Comput. Phys. Commun. **178**, 685 (2008).
[30]F. D. M. Haldane, Phys. Rev. Lett. **93**, 206602 (2004).
[31]H. Zhang, F. Freimuth, S. Blügel, Y. Mokrousov, and I. Souza, Phys. Rev. Lett. **106**, 117202 (2011).
[32]I. Souza, N. Marzari, and D. Vanderbilt, Phys. Rev. B **65**, 035109 (2001).
[33]This is in contrast to the case considered in Ref. 19, where states of the same spin character from the conduction and valence bands are pulled to the Fermi energy by increasing the spin-orbit strength.
[34]S. Murakami, N. Nagaosa, and S.-C. Zhang, Phys. Rev. Lett. **93**, 156804 (2004).
[35]B. A. Bernevig, T. L. Hughes, and S.-C. Zhang, Science **314**, 1757 (2006).
[36]M. König, S. Wiedmann, C. Brüne, A. Roth, H. Buhmann, L. W. Molenkamp, X.-L. Qi, and S.-C. Zhang, Science **318**, 766 (2007).
[37]L. Sheng, D. N. Sheng, C. S. Ting, and F. D. M. Haldane, Phys. Rev. Lett. **95**, 136602 (2005).
[38]R. Resta, Rev. Mod. Phys. **66**, 899 (1994).
[39]H. Jin, J. Im, and A. J. Freeman, Phys. Rev. B **84**, 134408 (2011).
[40]S. Heinze, Appl. Phys. A **85**, 407 (2006).
[41]H. Zhang, C. Lazo, S. Blügel, S. Heinze, and Y. Mokrousov, Phys. Rev. Lett. **108**, 056802 (2012).